2015 23rd Mediterranean Conference on Control and Automation (MED)
June 16-19, 2015. Torremolinos, Spain

Energy efficiency of underwater snake robot locomotion

E. Kelasidi, K. Y. Pettersen and J. T. Gravdahl

Abstract— **Energy efficiency is one of the main challenges for long-term autonomy of underwater robotic systems. In this paper, we present results regarding the power consumption of underwater snake robots. In particular, we investigate the relationship between the parameters of the gait patterns, the consumed energy and the forward velocity for different motion patterns for underwater snake robots. Based on a simulation study, we propose empirical rules to choose the parameters of the gait patterns, taking into account both the desired forward velocity and the power consumption of the system. The simulation results show that with respect to the cost of transportation metric, increasing the number of links the energy efficiency decreases for both lateral undulation and eel-like motion.**

Index Terms—**Underwater snake robots, energy consumption, energy efficiency of swimming robots.**

I. Introduction

The use of underwater vehicles has rapidly increased the last decades since these systems are able to operate in deeper and high risk areas which human beings cannot reach. As has been noted in the bio-robotics community, underwater swimming robots bring a promising prospective to improve the efficiency and maneuverability of next generation underwater vehicles [1]–[4]. They have several promising applications for underwater exploration, monitoring, surveillance and inspection, and they carry a lot of potential for inspection of subsea oil and gas installations. Also, for the biological community and marine archeology, snake robots that are able to swim smoothly without much noise, and that can navigate in difficult environments such as ship wrecks, are very interesting [1]. To realize operational snake robots for such underwater applications, a number of different control design challenges must first be solved. An important control problem concerns the ability to achieve efficient motion with preferably a minimal amount of consumed energy in order to be able to undertake longer missions, and this is the topic of this paper.

Studies of hyper-redundant mechanisms (HRMs) have largely restricted themselves to land-based studies, where several models for snake robots have been proposed [5]. Empirical and analytic studies of snake locomotion were reported by Gray [6], while the work of Hirose [7] is among the first attempts to develop a snake robot prototype. Comparing amphibious snake robots to the traditional land-based ones, the former have the advantage of adaptability to aquatic environments. Research on amphibious snake robots (also referred to as lamprey robots or eel-like robots) is, however, much less extensive than for the traditional types and fewer prototypes have been developed [8], [9]. Several results have been reported in the related field of design, modeling and control of underwater robots that mimic the movement of fish [10]. Regarding swimming snake robots, the underlying propulsive force generation mechanism has been studied through exploration of the fluid dynamics surrounding the body. In this field, several mathematical models of underwater snake robots have been proposed [1]–[4], [11]–[14].

In [1], the authors propose a model of underwater snake robots, where the dynamic equations are written in closed form. This modeling approach takes into account both the linear and the nonlinear drag forces (resistive fluid forces), the added mass effect (reactive fluid forces), the fluid moments and the current effects. Compared to the models in [2]–[4], [11]–[14] it is an advantage from an analysis point of view that the model is in closed form, as opposed to including numerical evaluations of the drag effects. In addition, it is beneficial that it includes both resistive and reactive fluid forces, since swimming snake robots operate at Reynolds numbers that require both these effects to be taken into account. Therefore, the analysis in this paper will be based on the dynamic model presented in [1]. We present in this paper simulation results in order to investigate the relationships between the parameters of the gait patterns, the consumed energy and the forward velocity for different motion patterns for underwater snake robots. This paper presents preliminary result by investigating the power consumption of different motion patterns for underwater snake robots and comparing the most efficient motion pattern depending on the desired motion. Based on the results of this investigation, we present empirical rules to choose the values for the parameters of the motion gait pattern of underwater snake robots. The purpose of this study is to investigate the issues that influence the performance of underwater snake robots, both when it comes to the achieved forward velocity (moving performance) and the energy efficiency (transportation performance). In particular, the energy index [15] is used in order to compare the energy efficiency of underwater snake robots for different motion patterns. A similar approach is used in order to indicate the relationship between the mechanical index and the energy index of different transformation modes for ships in [15]. Comparison

J. T. Gravdahl is with the Dept. of Engineering Cybernetics at NTNU, NO-7491 Trondheim, Norway. E-mail: Tommy.Gravdahl@itk.ntnu.no

E. Kelasidi, and K. Y. Pettersen are with the Centre for Autonomous Marine Operations and Systems, Dept. of Engineering Cybernetics at NTNU, NO-7491 Trondheim, Norway. E-mail: {Eleni.Kelasidi,Kristin.Y.Pettersen}@itk.ntnu.no

This work was partly supported by the Research Council of Norway through project no. 205622 and its Centres of Excellence funding scheme, project no. 223254-AMOS

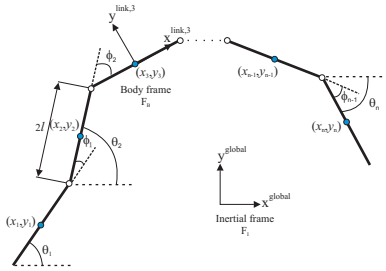

(a) Kinematic parameters

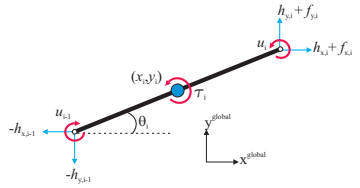

(b) Forces and torques acting on each link

Fig. 1: Underwater snake robot

results are obtained for the average power consumption and the cost of transportation of underwater snake robots for different motion patterns.

The paper is organized as follows. Section II presents the dynamic model and the motion pattern of an underwater snake robot. The energetics of underwater snake robots are presented in Section III, followed by simulation results in Section VI. Finally, conclusions and suggestions for further research are given in Section V.

II. Underwater snake robots

This section briefly presents a model of the kinematics and dynamics of an underwater snake robot moving in a virtual horizontal plane. A more detailed presentation of the model can be found in [1]. In addition, a general sinusoidal motion pattern proposed in [16] will be presented, and also a low-level joint controller is presented.

A. Notations and defined symbols

The underwater snake robot consists of n rigid links of equal length $2l$ interconnected by $n-1$ joints. The links are assumed to have the same mass m and moment of inertia $J=\frac{1}{3}ml^2$. The mass of each link is uniformly distributed so that the link CM (center of mass) is located at its center point (at length l from the joint at each side). The total mass of the snake robot is therefore nm. In the following sections, the kinematics and dynamics of the robot will be described in terms of the mathematical symbols described in Table I and illustrated in Fig. 1. The following vectors and matrices are used in the subsequent sections:

$$\mathbf{A}=\begin{bmatrix} 1 & 1 & & \\ & \ddots & \ddots & \\ & & 1 & 1 \end{bmatrix},\ \mathbf{D}=\begin{bmatrix} 1 & -1 & & \\ & \ddots & \ddots & \\ & & 1 & -1 \end{bmatrix},$$

where $\mathbf{A},\mathbf{D}\in\mathbb{R}^{(n-1)\times n}$. Furthermore,

$$\mathbf{e}=\begin{bmatrix} 1 & \dots & 1 \end{bmatrix}^T\in\mathbb{R}^n,\ \mathbf{E}=\begin{bmatrix} \mathbf{e} & \mathbf{0}_{n\times 1} \\ \mathbf{0}_{n\times 1} & \mathbf{e} \end{bmatrix}\in\mathbb{R}^{2n\times 2},$$

$$\begin{aligned} \mathbf{S}_\theta &= \operatorname{diag}(\sin\theta)\in\mathbb{R}^{n\times n}, \qquad \mathbf{C}_\theta=\operatorname{diag}(\cos\theta)\in\mathbb{R}^{n\times n} \\ \dot\theta^2 &= \begin{bmatrix} \dot\theta_1{}^2 & \dots & \dot\theta_n{}^2 \end{bmatrix}^T\in\mathbb{R}^n,\ \mathbf{J}=J\mathbf{I}_n,\ \mathbf{K}=\mathbf{A}^T\left(\mathbf{D}\mathbf{D}^T\right)^{-1}\mathbf{D} \end{aligned}$$

TABLE I: Definition of mathematical terms

Symbol	Description	Vector
n	The number of links	
l	The half length of a link	
m	Mass of each link	
J	Moment of inertia of each link	
θ_i	Angle between link i and the global x axis	$\theta\in\mathbb{R}^n$
ϕ_i	Angle of joint i	$\phi\in\mathbb{R}^{n-1}$
(x_i,y_i)	Global coordinates of the CM of link i	$\mathbf{X},\mathbf{Y}\in\mathbb{R}^n$
(p_x,p_y)	Global coordinates of the CM of the robot	$\mathbf{p}_{CM}\in\mathbb{R}^2$
u_i	Actuator torque of joint between link i and link $i+1$	$\mathbf{u}\in\mathbb{R}^{n-1}$
u_{i-1}	Actuator torque of joint between link i and link $i-1$	$\mathbf{u}\in\mathbb{R}^{n-1}$
$(f_{x,i},f_{y,i})$	Fluid force on link i	$\mathbf{f}_x,\mathbf{f}_y\in\mathbb{R}^n$
τ_i	Fluid torque on link i	$\tau\in\mathbb{R}^n$
$(h_{x,i},h_{y,i})$	Joint constraint force on link i from link $i+1$	$\mathbf{h}_x,\mathbf{h}_y\in\mathbb{R}^{n-1}$
$-(h_{x,i-1},h_{y,i-1})$	Joint constraint force on link i from link $i-1$	$\mathbf{h}_x,\mathbf{h}_y\in\mathbb{R}^{n-1}$

B. Kinematics of the underwater snake robot

The snake robot is assumed to move in a virtual horizontal plane, fully immersed in water, and has n+2 degrees of freedom (n links angles and the x-y position of the robot). The *link angle* of each link $i\in 1,\dots,n$ of the snake robot is denoted by $\theta_i\in\mathbb{R}$, while the *joint angle* of joint $i\in 1,\dots,n-1$ is given by $\phi_i=\theta_i-\theta_{i-1}$. The *heading* (or *orientation*) $\bar\theta\in\mathbb{R}$ of the snake is defined as the average of the link angles, i.e. as [5]

$$\bar\theta=\frac{1}{n}\sum_{i=1}^{n}\theta_i. \tag{1}$$

The global frame position $\mathbf{p}_{\mathrm{CM}}\in\mathbb{R}^2$ of the CM (center of mass) of the robot is given by

$$\mathbf{p}_{\mathrm{CM}}=\begin{bmatrix} p_x \\ p_y \end{bmatrix}=\begin{bmatrix} \frac{1}{nm}\sum_{i=1}^{n}mx_i \\ \frac{1}{nm}\sum_{i=1}^{n}my_i \end{bmatrix}=\frac{1}{n}\begin{bmatrix} \mathbf{e}^T\mathbf{X} \\ \mathbf{e}^T\mathbf{Y} \end{bmatrix}, \tag{2}$$

where (x_i,y_i) are the global frame coordinates of the CM of link i, $\mathbf{X}=[x_1,\dots,x_n]^T\in\mathbb{R}^n$ and $\mathbf{Y}=[y_1,\dots,y_n]^T\in\mathbb{R}^n$. The forward velocity of the robot is denoted by $\bar v_t\in\mathbb{R}$ and is defined as the component of the CM velocity along the current heading of the snake, i.e.

$$\bar v_t=\dot p_x\cos\bar\theta+\dot p_y\sin\bar\theta. \tag{3}$$

C. Hydrodynamic modeling

As has been noted in the bio-robotics community, underwater snake (eel-like) robots bring a promising prospective to improve the efficiency and maneuverability of next generation underwater vehicles. The dynamic modeling of the contact forces is, however, quite complicated compared to the modeling of the overall rigid motion. In [1] it is shown that the fluid forces on all links can be expressed in vector form as

$$\mathbf{f}=\begin{bmatrix} \mathbf{f_x} \\ \mathbf{f_y} \end{bmatrix}=\begin{bmatrix} \mathbf{f_{A_x}} \\ \mathbf{f_{A_y}} \end{bmatrix}+\begin{bmatrix} \mathbf{f^I_{D_x}} \\ \mathbf{f^I_{D_y}} \end{bmatrix}+\begin{bmatrix} \mathbf{f^{II}_{D_x}} \\ \mathbf{f^{II}_{D_y}} \end{bmatrix}. \tag{4}$$

The vectors $\mathbf{f_{A_x}}$ and $\mathbf{f_{A_y}}$ represent the effects from added mass forces and are expressed as

$$\begin{aligned} \begin{bmatrix} \mathbf{f_{A_x}} \\ \mathbf{f_{A_y}} \end{bmatrix} &= -\begin{bmatrix} \mu_n(\mathbf{S}_\theta)^2 & -\mu_n\mathbf{S}_\theta\mathbf{C}_\theta \\ -\mu_n\mathbf{S}_\theta\mathbf{C}_\theta & \mu_n(\mathbf{C}_\theta)^2 \end{bmatrix}\begin{bmatrix} \ddot{\mathbf{X}} \\ \ddot{\mathbf{Y}} \end{bmatrix} \\ &\quad -\begin{bmatrix} -\mu_n\mathbf{S}_\theta\mathbf{C}_\theta & -\mu_n(\mathbf{S}_\theta)^2 \\ \mu_n(\mathbf{C}_\theta)^2 & \mu_n\mathbf{S}_\theta\mathbf{C}_\theta \end{bmatrix}\begin{bmatrix} \mathbf{V}_x^a \\ \mathbf{V}_y^a \end{bmatrix}\dot\theta, \end{aligned} \tag{5}$$

where $\mathbf{V}_x^a=\operatorname{diag}(V_{x,1},\dots,V_{x,n})\in\mathbb{R}^{n\times n}$, $\mathbf{V}_y^a=\operatorname{diag}(V_{y,1},\dots,V_{y,n})\in\mathbb{R}^{n\times n}$ and $[V_{x,i},V_{y,i}]^T$ is the current velocity expressed in inertial frame coordinates. The vectors $\mathbf{f^I_{D_x}}$, $\mathbf{f^I_{D_y}}$ and $\mathbf{f^{II}_{D_x}}$, $\mathbf{f^{II}_{D_y}}$ present the effects from the linear (6) and nonlinear drag forces (7), respectively, where the relative velocities are given by (8).

$$\begin{bmatrix} \mathbf{f^I_{D_x}} \\ \mathbf{f^I_{D_y}} \end{bmatrix}=-\begin{bmatrix} c_t(\mathbf{C}_\theta)^2+c_n(\mathbf{S}_\theta)^2 & (c_t-c_n)\mathbf{S}_\theta\mathbf{C}_\theta \\ (c_t-c_n)\mathbf{S}_\theta\mathbf{C}_\theta & c_t(\mathbf{S}_\theta)^2+c_n(\mathbf{C}_\theta)^2 \end{bmatrix}\begin{bmatrix} \dot{\mathbf{X}}-\mathbf{V}_x \\ \dot{\mathbf{Y}}-\mathbf{V}_y \end{bmatrix} \tag{6}$$

$$\begin{bmatrix} \mathbf{f}^{\mathrm{II}}_{\mathbf{Dx}} \\ \mathbf{f}^{\mathrm{II}}_{\mathbf{Dy}} \end{bmatrix} = -\begin{bmatrix} c_t\mathbf{C}_\theta & -c_n\mathbf{S}_\theta \\ c_t\mathbf{S}_\theta & c_n\mathbf{C}_\theta \end{bmatrix} \mathrm{sgn}\left(\begin{bmatrix} \mathbf{V_{r_x}} \\ \mathbf{V_{r_y}} \end{bmatrix}\right) \begin{bmatrix} \mathbf{V_{r_x}}^2 \\ \mathbf{V_{r_y}}^2 \end{bmatrix} \tag{7}$$

$$\begin{bmatrix} \mathbf{V_{r_x}} \\ \mathbf{V_{r_y}} \end{bmatrix} = \begin{bmatrix} \mathbf{C}_\theta & \mathbf{S}_\theta \\ -\mathbf{S}_\theta & \mathbf{C}_\theta \end{bmatrix} \begin{bmatrix} \dot{\mathbf{X}} - \mathbf{V}_x \\ \dot{\mathbf{Y}} - \mathbf{V}_y \end{bmatrix} \tag{8}$$

In addition, the fluid torques on all links are

$$\tau = -\Lambda_1\ddot{\theta} - \Lambda_2\dot{\theta} - \Lambda_3\dot{\theta}|\dot{\theta}|, \tag{9}$$

where $\Lambda_1 = \lambda_1\mathbf{I}_n$, $\Lambda_2 = \lambda_2\mathbf{I}_n$ and $\Lambda_3 = \lambda_3\mathbf{I}_n$. The coefficients c_t, c_n, λ_2, λ_3 represent the drag forces parameters due to the pressure difference between the two sides of the body, and the parameters μ_n, λ_1 represent the added mass of the fluid carried by the moving body.

D. Equations of motion

This section presents the equations of motion for the underwater snake robot. In [1], it is shown that the acceleration of the CM may be expressed as

$$\begin{aligned} \begin{bmatrix} \ddot{p}_x \\ \ddot{p}_y \end{bmatrix} &= -\mathbf{M}_p \begin{bmatrix} \mathbf{e}^T\mu_n\mathbf{S}_\theta^2 & -\mathbf{e}^T\mu_n\mathbf{S}_\theta\mathbf{C}_\theta \\ -\mathbf{e}^T\mu_n\mathbf{S}_\theta\mathbf{C}_\theta & \mathbf{e}^T\mu_n\mathbf{C}_\theta^2 \end{bmatrix} \begin{bmatrix} l\mathbf{K}^T(\mathbf{C}_\theta\dot{\theta}^2 + \mathbf{S}_\theta\ddot{\theta}) \\ l\mathbf{K}^T(\mathbf{S}_\theta\dot{\theta}^2 - \mathbf{C}_\theta\ddot{\theta}) \end{bmatrix} \\ &- \mathbf{M}_p \begin{bmatrix} -\mathbf{e}^T\mu_n\mathbf{S}_\theta\mathbf{C}_\theta & -\mathbf{e}^T\mu_n\mathbf{S}_\theta^2 \\ \mathbf{e}^T\mu_n\mathbf{C}_\theta^2 & \mathbf{e}^T\mu_n\mathbf{S}_\theta\mathbf{C}_\theta \end{bmatrix} \begin{bmatrix} \mathbf{V}_x^a \\ \mathbf{V}_y^a \end{bmatrix} \dot{\theta} + \mathbf{M}_p \begin{bmatrix} \mathbf{e}^T\mathbf{f_{Dx}} \\ \mathbf{e}^T\mathbf{f_{Dy}} \end{bmatrix} \end{aligned} \tag{10}$$

where

$$\mathbf{M}_p = \begin{bmatrix} m_{11} & m_{12} \\ m_{21} & m_{22} \end{bmatrix} = \begin{bmatrix} nm + \mathbf{e}^T\mu_n\mathbf{S}_\theta^2\mathbf{e} & -\mathbf{e}^T\mu_n\mathbf{S}_\theta\mathbf{C}_\theta\mathbf{e} \\ -\mathbf{e}^T\mu_n\mathbf{S}_\theta\mathbf{C}_\theta\mathbf{e} & nm + \mathbf{e}^T\mu_n\mathbf{C}_\theta^2\mathbf{e} \end{bmatrix}^{-1}. \tag{11}$$

and $\mathbf{f_{Dx}} = \mathbf{f}^{\mathrm{I}}_{\mathbf{D_x}} + \mathbf{f}^{\mathrm{II}}_{\mathbf{D_x}}$ and $\mathbf{f_{Dy}} = \mathbf{f}^{\mathrm{I}}_{\mathbf{D_y}} + \mathbf{f}^{\mathrm{II}}_{\mathbf{D_y}}$ are the drag forces in x and y directions. In addition, it is shown that [1] the model of an underwater snake robot may be expressed as

$$\mathbf{M}_\theta\ddot{\theta} + \mathbf{W}_\theta\dot{\theta}^2 + \mathbf{V}_\theta\dot{\theta} + \Lambda_3|\dot{\theta}|\dot{\theta} + \mathbf{K_{Dx}}\mathbf{f_{Dx}} + \mathbf{K_{Dy}}\mathbf{f_{Dy}} = \mathbf{D}^T\mathbf{u}, \tag{12}$$

where $\mathbf{M}_\theta$, $\mathbf{W}_\theta$, $\mathbf{V}_\theta$, $\mathbf{K_{Dx}}$ and $\mathbf{K_{Dy}}$ are defined as

$$\mathbf{M}_\theta = \mathbf{J} + ml^2\mathbf{S}_\theta\mathbf{V}\mathbf{S}_\theta + ml^2\mathbf{C}_\theta\mathbf{V}\mathbf{C}_\theta + \Lambda_1 + l^2\mu_n\mathbf{K}_1\mathbf{K}^T\mathbf{S}_\theta + l^2\mu_n\mathbf{K}_2\mathbf{K}^T\mathbf{C}_\theta \tag{13}$$

$$\mathbf{W}_\theta = ml^2\mathbf{S}_\theta\mathbf{V}\mathbf{C}_\theta - ml^2\mathbf{C}_\theta\mathbf{V}\mathbf{S}_\theta + l^2\mu_n\mathbf{K}_1\mathbf{K}^T\mathbf{C}_\theta - l^2\mu_n\mathbf{K}_2\mathbf{K}^T\mathbf{S}_\theta \tag{14}$$

$$\mathbf{V}_\theta = \Lambda_2 - l\mu_n\mathbf{K}_2\mathbf{V}_x^a - l\mu_n\mathbf{K}_1\mathbf{V}_y^a \tag{15}$$

$$\mathbf{K_{Dx}} = l\mu_n m_{11}A_1\mathbf{e}\mathbf{e}^T - l\mu_n m_{21}A_2\mathbf{e}\mathbf{e}^T - l\mathbf{S}_\theta\mathbf{K} \tag{16}$$

$$\mathbf{K_{Dy}} = l\mu_n m_{12}A_1\mathbf{e}\mathbf{e}^T - l\mu_n m_{22}A_2\mathbf{e}\mathbf{e}^T + l\mathbf{C}_\theta\mathbf{K} \tag{17}$$

where $\mathbf{K}_1 = \mathbf{A}_1 + \mu_n\mathbf{A}_1\mathbf{e}\mathbf{e}^T(m_{12}\mathbf{S}_\theta\mathbf{C}_\theta - m_{11}\mathbf{S}_\theta^2) - \mu_n\mathbf{A}_2\mathbf{e}\mathbf{e}^T(m_{22}\mathbf{S}_\theta\mathbf{C}_\theta - m_{21}\mathbf{S}_\theta^2)$, $\mathbf{K}_2 = \mathbf{A}_2 - \mu_n\mathbf{A}_1\mathbf{e}\mathbf{e}^T(m_{11}\mathbf{S}_\theta\mathbf{C}_\theta - m_{12}\mathbf{C}_\theta^2) + \mu_n\mathbf{A}_2\mathbf{e}\mathbf{e}^T(m_{21}\mathbf{S}_\theta\mathbf{C}_\theta - m_{22}\mathbf{C}_\theta^2)$, $\mathbf{A}_1 = \mathbf{S}_\theta\mathbf{K}\mathbf{S}_\theta^2 + \mathbf{C}_\theta\mathbf{K}\mathbf{S}_\theta\mathbf{C}_\theta$, $\mathbf{A}_2 = \mathbf{S}_\theta\mathbf{K}\mathbf{S}_\theta\mathbf{C}_\theta + \mathbf{C}_\theta\mathbf{K}\mathbf{C}_\theta^2$.

In summary, the equations of motion for the underwater snake robot are given by (10) and (12). By introducing the state variable $\mathbf{x} = \left[\theta^T, \mathbf{p}_{CM}^T, \dot{\theta}^T, \dot{\mathbf{p}}_{CM}^T\right]^T \in \mathbb{R}^{2n+4}$, we can rewrite the model of the robot compactly in state space form as

$$\dot{\mathbf{x}} = \left[\dot{\theta}^T, \dot{\mathbf{p}}_{CM}^T, \ddot{\theta}^T, \ddot{\mathbf{p}}_{CM}^T\right]^T = \mathbf{F}(\mathbf{x}, \mathbf{u}) \tag{18}$$

where the elements of $\mathbf{F}(\mathbf{x}, \mathbf{u})$ are found by solving (10) and (12) for $\ddot{\mathbf{p}}_{CM}$ and $\ddot{\theta}$, respectively.

E. Motion Pattern

Previous studies on swimming snake robots have focused on two motion patterns; lateral undulation and eel-like motion. In this paper, we will use a general sinusoidal motion pattern that describes a broader class of motion patterns including lateral undulation and eel-like motion [16]. A general sinusoidal motion pattern can be achieved by making each joint $i \in \{1, \cdots, n-1\}$ of the underwater snake robot track the sinusoidal reference signal

$$\phi_i^*(t) = \alpha\mathrm{g}(i,n)\sin(\omega t + (i-1)\delta) + \gamma, \tag{19}$$

where α and ω are the maximum amplitude and the frequency, respectively, δ determines the phase shift between the joints, while the function $\mathrm{g}(i,n)$ is a scaling function for the amplitude of joint i which allows (19) to describe a quite general class of sinusoidal functions, including several different snake motion patterns. For instance, $\mathrm{g}(i,n) = 1$ gives lateral undulation, while $\mathrm{g}(i,n) = (n-i)/(n+1)$ gives eel-like motion. The parameter γ is a joint offset coordinate that can be used to control the direction of the locomotion [1]. In particular, in [5] and [17], γ is shown to affect the direction of locomotion in the case of land-based snake robots and fish robots, respectively.

F. Low-level joint control

A PD-controller is used to calculate the joints' actuator torques from the joints' reference angles according to

$$u_i = \ddot{\phi}_i^* + K_{p,i}(\phi_i^* - \phi_i) + K_{d,i}(\dot{\phi}_i^* - \dot{\phi}_i), \quad i = 1, \ldots, n-1, \tag{20}$$

where $K_{p,i} > 0$ and $K_{d,i} > 0$ are the gains of the controller.

III. Energy consumption

In this section, we will present the energy consumption analysis approach that is applied for the underwater snake robots. In addition, we will present a cost of transportation metric that makes it possible to obtain comparison results of the consumed energy for different systems (e.g. underwater snake robots with different number of links and mass).

A. Energetics of underwater snake robots

For underwater snake robots, the propulsion is generated by the motion of the joints and its interaction with the surrounding fluid. The actuator torque input to the joints is thus transformed into a combination of joint motion and energy that is dissipated by the fluid. We assume that we have perfect joints and thus the total amount of energy of the system (E_{s}) generated by this input is the sum of kinetic energy (E_{kinetic}) and the energy that is dissipated to the surrounding fluid (E_{fluid}) [14], [15]. The sum of these two is thus the total energy that is spent for the propulsion of the robot.

$$E_{\mathrm{s}} = E_{\mathrm{kinetic}} + E_{\mathrm{fluid}} \tag{21}$$

where E_{s} is given by

$$E_{\mathrm{s}} = \int_0^T \left(\sum_{i=1}^{n-1} u_i(t)\dot{\phi}_i(t)\right) dt. \tag{22}$$

T is the time that corresponds to a complete swimming cycle, u_i is the actuation torque of joint i given by (20) and $\dot{\phi}_i$ is the joint's angular velocity defined as $\dot{\phi}_i = \dot{\theta}_i - \dot{\theta}_{i-1}$.

For a complete swimming cycle, T, the averaged power consumption, P_{avg}, is calculated as follows

$$P_{\mathrm{avg}} = \frac{1}{T}\int_0^T \left(\sum_{i=1}^{n-1} u_i(t)\dot{\phi}_i(t)\right) dt. \tag{23}$$

B. Efficient Motion

For underwater applications, it is important to find an optimum combination of different underwater vehicles or different motion modes, which lead to the lowest energy consumption. To compare the energy consumption of different vehicles, we need a suitable basis for comparison. In this study, in order to compare vehicles with different dimensions and characteristics, a dimensionless quantity is used. Generally, the energy index (cost of transportation) quantifies the energy efficiency of a vehicle, or of a robotic system in our case, from one place to another. The cost of

transportation has been used in a wide range of applications in order to define the most energy efficient motion of different systems [15]. In this study, the cost of transportation is defined as

$$COT = \frac{\text{Energy}}{\text{Mass} \times g \times \text{Distance}}. \quad (24)$$

Cost of transportation is non-dimensional and it quantifies how much energy is applied to a system of a specified mass in order to move the system a defined distance (the ratio between the consumed energy and the transferred weight times the covered distance). Using the energy index approach, the vehicle is operated without taking into account the kind of propulsion system that is implemented inside. This coefficient is useful for the comparison of different types of transportation, since it gives an indication of the required power to a system and the effective power. A similar approach is used in order to indicate the relationship between the mechanical index and the energy index of different transformation modes for ships in [15]. In particular, the purpose of the case study in [15] was to investigate the issues that could influence both the moving performance and the transportation performance of ships. In this paper, we will use the energy index in order to investigate the energy efficiency of underwater snake robots with different links.

IV. Simulation Study

In this section, simulation results will be presented for underwater snake robots moving a distance of 4 m for both lateral undulation and eel-like motion patterns. Note that these results are derived for zero current velocity. In this initial study, the current effects have not been considered. The models were implemented in *Matlab R2013b*. The dynamics was calculated using the *ode23tb* solver with a relative and absolute error tolerance of 10^{-4}.

A. Simulation parameters

We consider snake robots with respectively $n = 5$, $n = 10$, $n = 20$ links, each one having length $2l = 2 \times 0.14$ m. The five links constitutes a rather short snake robot, while ten to twenty links constitute a more normal length of snake robots. The mass of each link is $m = 0.6597$ kg and is chosen so to fulfil the neutrally buoyant assumption. The initial values of the states of the snake robot were set to initial reference values at $t = 0$ with its heading along the inertial x axis. The hydrodynamic parameters are $c_t = 0.2639$, $c_n = 8.4$, $\mu_n = 0.3958$, $\lambda_1 = 2.298810^{-7}$, $\lambda_2 = 4.310310^{-4}$ and $\lambda_3 = 2.262910^{-5}$. An extensive discussion about the values of the fluid parameters can be found in [1]. The joint PD controller (20) is used for each joint with parameters $k_p = 200$, $k_d = 5$, and lateral undulation and eel-like motion are achieved by choosing $\mathrm{g}(i,n) = 1$ and $\mathrm{g}(i,n) = (n-i)/(n+1)$, respectively. It should be noted that the anisotropic friction property that is needed for forward locomotion [1], is achieved by a low drag coefficient in the tangential direction and a higher one in the perpendicular. The gait pattern parameters are presented in each simulation result.

B. Simulation results

Simulation results are presented for lateral undulation and eel-like motion pattern for the underwater snake robots of different lengths. In particular, simulation results for the forward velocity $\bar{v}_t$, the averaged power consumption, P_{avg}, and the cost of transportation for a constant amplitude $\alpha = 20^o$ are presented for lateral undulation and eel-like motion in Fig. 2 and Fig. 3, respectively. Fig. 2a and Fig. 3a show that by increasing the phase shift δ there is an increase of the forward velocity until a value of δ_{max} where the system reaches the maximum velocity. After this value, an additional increase of this parameter causes a decrease in the forward velocity. It is worth noting that, for different values of ω, the forward velocity has a similar behavior, and that δ_{max} is approximately the same for all values of omega. In addition, we see that for different number of links, n, the value of δ_{max} is not the same. Increasing the number of the links, we see that δ_{max} decreases, and also that the maximum velocity reached at δ_{max} increases. The δ_{max} values for $n = 5$, $n = 10$ and $n = 20$ links are $\delta_{max} = 30^o$, $\delta_{max} = 20^o$ and $\delta_{max} = 20^o$ respectively, for lateral undulation (Fig. 2a) and $\delta_{max} = 40^o$, $\delta_{max} = 20^o$ and $\delta_{max} = 10^o$ for eel-like motion (Fig. 3a), for almost all values of ω except the very high frequency values. Note that for $n = 10$ and $n = 20$ links the maximum phase shift δ_{max} has the same value (Fig. 2a), which shows that for $n > 10$, we can choose $\delta_{max} = 20^o$ in order to reach the maximum forward velocity.

From Fig. 2b and Fig. 3b, we see that the average power consumption is decreasing by increasing δ, while also the cost of transportation is decreasing (Fig. 2c and Fig. 3c) for both lateral undulation and eel-like motion patterns. In addition, we can see that for δ_{max}, which makes the robot reach the maximum velocity, an additional increment of the δ does not significantly affect the cost of transportation, in particular for the longer snake robots. The cost of transportation actually increases a little for high values of δ. Furthermore, Fig. 2b and Fig. 2c show that the average power consumption increases and the motion of the system is less energy efficient when the frequency ω increases. Thus, we see that when choosing the parameter ω there is a trade-off between the maximum velocity on the one side and the power consumption and cost of transportation on the other. The discussion above indicates that for a constant value of the amplitude, a good choice of parameters is $\delta = \delta_{max}$. In particular, it is more efficient to make the compromise by choosing the values of δ and ω to reach a desired maximum speed of the robot while simultaneously we minimize the cost of transportation. In addition, we can easily conclude that smaller values than δ_{max} should not been considered since for these values the averaged power consumption is increased, the robot does not reach the maximum velocity, and the motion is less energy efficient. Furthermore, the frequency ω should be chosen as a trade-off between maximum forward velocity and power consumption.

Simulation results for the forward velocity $\bar{v}_t$, the averaged power consumption, P_{avg}, and the cost of transportation for a constant frequency $\omega = 70^o/\text{s}$ are presented for lateral undulation and eel-like motion in Fig. 4 and Fig. 5, respectively. From Fig. 4a and Fig. 5a, we can see that increasing the amplitude parameter α the robots manage to move faster, and

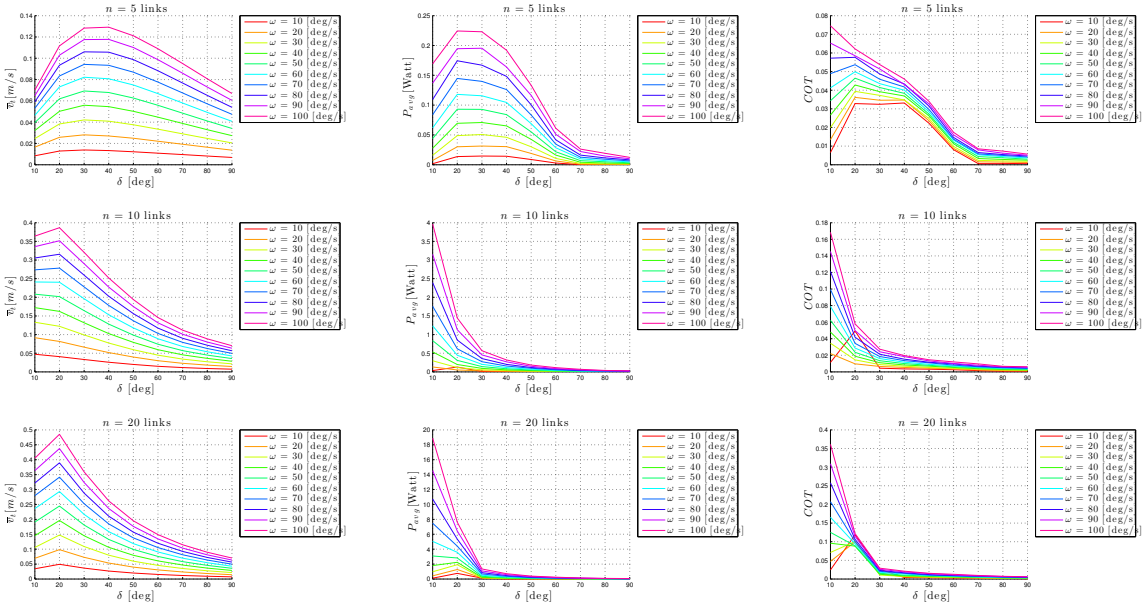

(a) Forward velocity (b) Averaged power consumption (c) Cost of transportation

Fig. 2: Simulation results for the lateral undulation motion pattern with constant amplitude $\alpha = 20^o$.

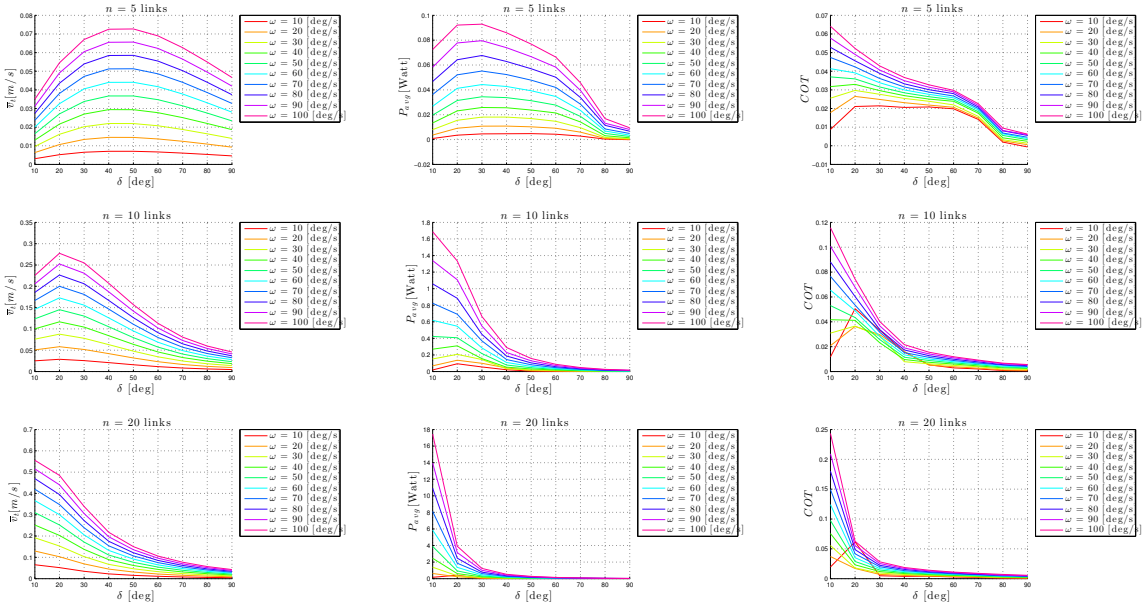

(a) Forward velocity (b) Averaged power consumption (c) Cost of transportation

Fig. 3: Simulation results for the eel-like motion pattern with constant amplitude $\alpha = 20^o$.

also that increasing the parameter α increases the average power consumption (Fig. 4b and Fig. 5b). Fig. 4a and Fig. 5a show that also keeping the frequency constant and varying the amplitude α, there exists a δ_{max} that gives a maximum forward velocity, and comparing Fig. 2a to 4a and Fig. 3a to 5a we see that the value of δ_{max} is the same for $\alpha > 20^o$. Fig. 4c and Fig. 5c show that for both lateral undulation and eel-like motion patterns, if we choose $\delta = \delta_{max}$ to get the maximum velocity then the cost of transportation is almost the same for all values of α. Hence, we can conclude that for a constant value of $\omega = 70^o/\text{s}$ and for $\delta = \delta_{max}$, we can choose the value of α in order to maximize the forward velocity of the robot and still keep the energy efficiency of the system.

In Fig. 6 and Fig. 7, simulation results for the forward velocity $\bar{v}_t$, the averaged power consumption, P_{avg}, and the cost of transportation for specified phase offset values $\delta = 35^o$, $\delta = 15^o$ and $\delta = 15^o$ for $n = 5$, $n = 10$ and

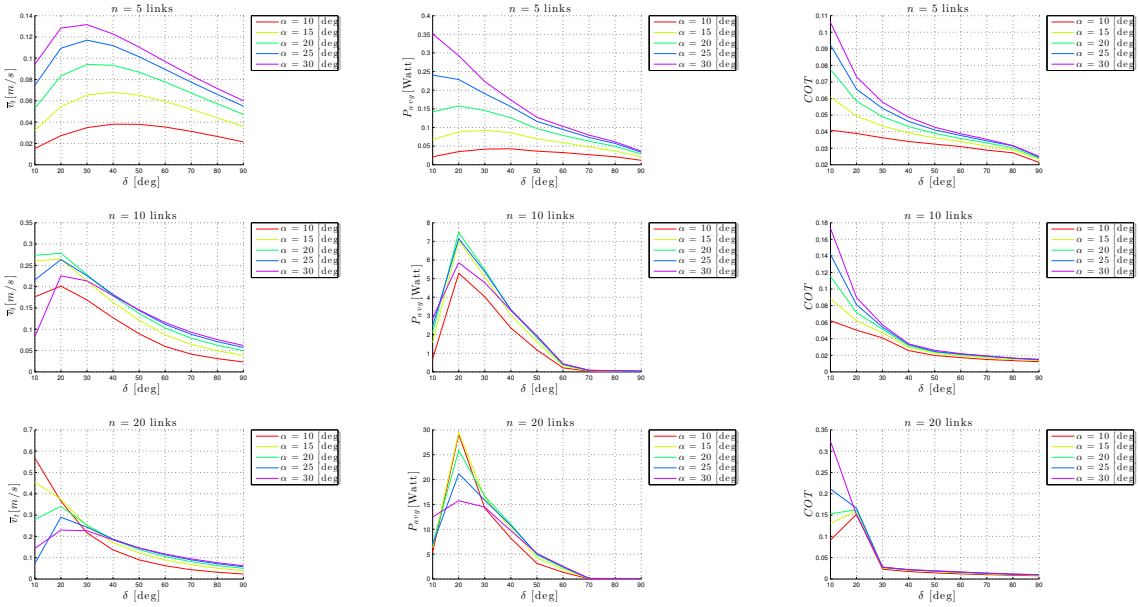

(a) Forward velocity (b) Averaged power consumption (c) Cost of transportation

Fig. 4: Simulation results for the lateral undulation motion pattern with constant frequency $\omega = 70^o/\text{s}$.

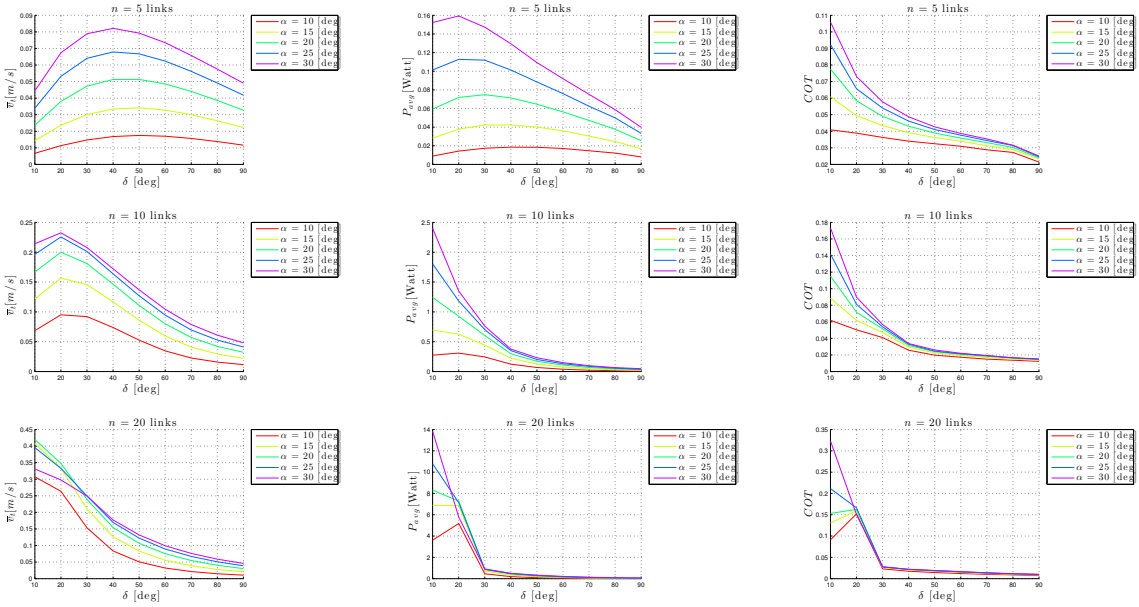

(a) Forward velocity (b) Averaged power consumption (c) Cost of transportation

Fig. 5: Simulation results for the eel-like motion pattern with constant frequency $\omega = 70^o/\text{s}$.

$n = 20$ links, are presented for lateral undulation and eel-like motion, respectively. From Fig. 6a and Fig. 7a, we can see that by increasing the parameter ω the forward velocity is increasing. In particular, the forward velocity is almost linearly increasing with the frequency ω for all different values of α. It is interesting to note, however, that the forward velocity increases with increasing amplitudes α for the short snake robot, while as the number of links increase, this is inversed such that for $n = 20$ links the forward velocity decreases with increasing amplitudes α. This show us that for a normal length snake robot of 10 links or more, we need to choose smaller values of the α to achieve the highest forward velocity of the system. Hence the forward velocity given a constant ω and a constant δ depends on the amplitude of the motion pattern and the number of the links. However, we can see that the average power consumption (Fig. 6b and Fig. 7b) increases when increasing the parameters α and ω. The cost of transportation presented in Fig. 6c and Fig. 7c

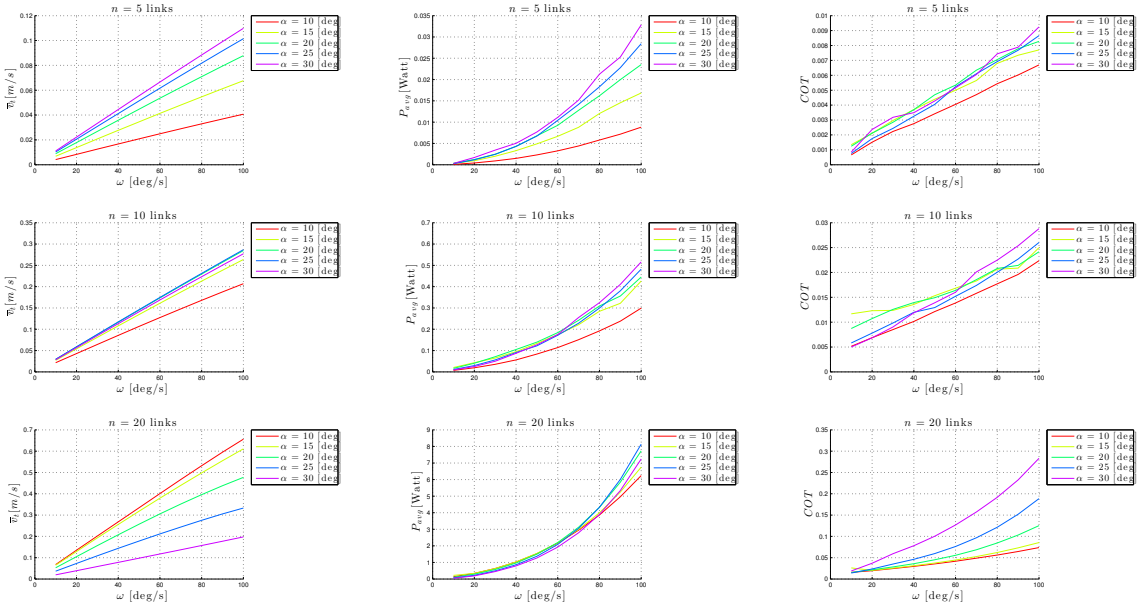

(a) Forward velocity (b) Averaged power consumption (c) Cost of transportation

Fig. 6: Simulation results for the lateral undulation motion pattern with specified phase offset $\delta = 35^o, 15^o, 15^o$.

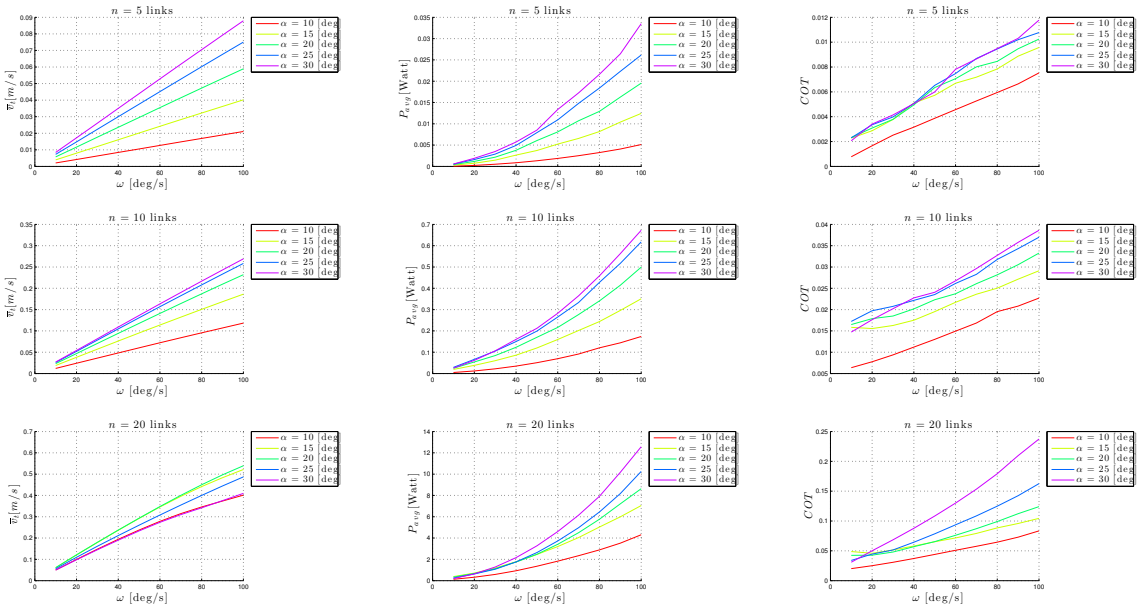

(a) Forward velocity (b) Energy consumption (c) Cost of transportation

Fig. 7: Simulation results for the eel-like motion pattern with specified phase offset $\delta = 35^o, 15^o, 15^o$.

for lateral undulation and eel-like motion show that the cost of transportation increases when increasing the parameter ω and by increasing the amplitude α.

From Fig. 2c-Fig. 7c, we see that by increasing the number of the links the cost of transportation is increased for both lateral undulation and eel-like motion. This higher cost of transportation of underwater snake robots for high number of actuation points were expected since by increasing the number of the links we need $n-1$ servo motors for the joint actuation. In order to reduce the actuation points and thus increase the energy efficiency, the underwater swimming robots should adapt not only the shape and the motion patterns of the biological fish but, in addition, the actuation strategies and the compliant bodies properties should be considered.

Now, we can summarize the empirical rules that can be used in order to choose the parameters of the gait patterns for underwater snake robots to achieve energy efficient motion

while reaching the fastest possible forward velocity based on the previous analysis.

Property 1: Given an underwater snake robot with n links described by (10,12) which is controlled by applying the joints' actuator torques as given in (20) with the joints' reference angles given by (19). When α is kept constant, the forward velocity increases by increasing the parameter ω. Furthermore, the forward velocity increases with increasing δ for $\delta < \delta_{max}$, and decreases with δ when $\delta > \delta_{max}$. The maximum forward velocity is achieved when $\delta = \delta_{max}$ as long as α and ω are constant.

Property 2: Given an underwater snake robot with n links described by (10,12) which is controlled by applying the joints' actuator torques as given in (20) with the joints' reference angles given by (19). The averaged power consumption decreases by increasing the parameter δ as long as α and ω are constant, and it increases by increasing the parameter ω as long as α and δ are constant.

Property 3: Given an underwater snake robot with n links described by (10,12) which is controlled by applying the joints' actuator torques as given in (20) with the joints' reference angles given by (19). The forward velocity increases by increasing the parameter α as long as ω is constant. The forward velocity is increasing with δ when $\delta < \delta_{max}$, and decreases with δ when $\delta > \delta_{max}$. The forward velocity has a maximum for $\delta = \delta_{max}$ as long as α and ω are constant.

Property 4: Given an underwater snake robot with n links described by (10,12) which is controlled by applying the joints' actuator torques as given in (20) with the joints' reference angles given by (19). The averaged power consumption decreases by increasing the parameter δ as long as α and ω are constant and increases by increasing the parameter α as long as ω and δ are constant.

Property 5: Given an underwater snake robot with n links described by (10,12) which is controlled by applying the joints' actuator torques as given in (20) with the joints' reference angles given by (19). When δ is constant, the forward velocity increases by increasing the parameter ω and α as long as δ is constant.

Property 6: Given an underwater snake robot with n links described by (10,12) which is controlled by applying the joints' actuator torques as given in (20) with the joints' reference angles given by (19). For a constant value of δ, the averaged power consumption increases by increasing the parameter ω and by increasing the amplitude α.

V. Conclusions

In this study, we have studied the energy efficiency of underwater snake robots. We have investigated the relationships between the parameters of the gait patterns, and the forward velocity, averaged power consumption, and cost of transportation for different motion patterns. Based on this, empirical rules are given to choose the gait pattern parameters, taking into account both the desired forward velocity and the energy efficiency of the snake robot. Furthermore, in order to compare the energy efficiency of snake robots different number of links, thus having different length and mass, a simulation study was performed comparing the energy consumption and the cost of transportation of different underwater snake robots.

The results of this study should be extended further by investigating other motion patterns for underwater snake robots in order to improve the mechanical design and the energy efficiency of underwater vehicles. Furthermore, the study has shown that there are direct and interesting relationships between the achievable forward velocity and the energy efficiency of the underwater snake robots, and the parameters of their gait pattern, and that this presents a multi-objective optimization problem. In future work, the authors will use optimization techniques in order to obtain the most suitable parameters of the motion patterns in order to increase the efficiency of the underwater swimming vehicle.

References

[1] E. Kelasidi, K. Y. Pettersen, J. T. Gravdahl, and P. Liljebäck, "Modeling of underwater snake robots," in *Proc. IEEE International Conference on Robotics and Automation (ICRA)*, Hong Kong, China, May 31 - June 7 2014, pp. 4540–4547.

[2] K. McIsaac and J. Ostrowski, "Motion planning for anguilliform locomotion," *IEEE Transactions on Robotics and Automation*, vol. 19, no. 4, pp. 637–625, 2003.

[3] F. Boyer, M. Porez, and W. Khalil, "Macro-continuous computed torque algorithm for a three-dimensional eel-like robot," *IEEE Transactions on Robotics*, vol. 22, no. 4, pp. 763 –775, aug. 2006.

[4] W. Khalil, G. Gallot, and F. Boyer, "Dynamic modeling and simulation of a 3-D serial eel-like robot," *IEEE Transactions on Systems, Man, and Cybernetics, Part C: Applications and Reviews*, vol. 37, no. 6, pp. 1259 –1268, Nov. 2007.

[5] P. Liljebäck, K. Y. Pettersen, Ø. Stavdahl, and J. T. Gravdahl, *Snake Robots: Modelling, Mechatronics, and Control*. Springer-Verlag, Advances in Industrial Control, 2013.

[6] J. Gray, "Studies in animal locomotion," *Journal of Experimental Biology*, vol. 10, no. 1, pp. 88–104, 1933.

[7] S. Hirose, *Biologically Inspired Robots: Snake-Like Locomotors and Manipulators*. Oxford: Oxford University Press, 1993.

[8] A. Crespi, A. Badertscher, A. Guignard, and A. Ijspeert, "Swimming and crawling with an amphibious snake robot," in *Proc. IEEE International Conference on Robotics and Automation (ICRA)*, April 2005, pp. 3024 – 3028.

[9] H. Yamada, S. Chigisaki, M. Mori, K.Takita, K. Ogami, and S. Hirose, "Development of amphibious snake-like robot ACM-R5," in *36th International Symposium on Robotics*, Tokyo, Japan, November 29-December 1 2005.

[10] J. Colgate and K. Lynch, "Mechanics and control of swimming: a review," *IEEE Journal of Oceanic Engineering*, vol. 29, no. 3, pp. 660 – 673, July 2004.

[11] G. Taylor, "Analysis of the swimming of long and narrow animals," *Proceedings of the Royal Society of London. Series A. Mathematical and Physical Sciences*, vol. 214, no. 1117, pp. 158–183, 1952.

[12] M. J. Lighthill, "Large-amplitude elongated-body theory of fish locomotion," *Proceedings of the Royal Society of London. Series B. Biological Sciences*, vol. 179, no. 1055, pp. 125–138, 1971.

[13] J. Chen, W. O. Friesen, and T. Iwasaki, "Mechanisms underlying rhythmic locomotion: bodyfluid interaction in undulatory swimming," *The Journal of Experimental Biology*, vol. 214, no. 4, pp. 561–574, 2011.

[14] A. Wiens and M. Nahon, "Optimally efficient swimming in hyper-redundant mechanisms: control, design, and energy recovery," *Bioinspir Biomim*, vol. 7, no. 4, p. 046016, 2012.

[15] W. Shi, D. Stapersma, and H. Grimmelius, "Comparison study on moving and transportation performance of transportation modes," *International journal of energy and environment*, vol. 2, 2008.

[16] E. Kelasidi, K. Y. Pettersen, and J. T. Gravdahl, "Stability analysis of underwater snake robot locomotion based on averaging theory," in *Proc. IEEE International Conference on Robotics and Biomimetics*, Bali, Indonesia, Dec. 5-10 2014.

[17] J. Guo, "A waypoint-tracking controller for a biomimetic autonomous underwater vehicle," *Ocean Engineering*, vol. 33, pp. 2369 – 2380, 2006.